Cellulose (2023) 30:2951–2967
https://doi.org/10.1007/s10570-023-05058-2

ORIGINAL RESEARCH

TEMPO-oxidized cellulose nanofibril/polyvalent cations hydrogels: a multifaceted view of network interactions and inner structure

Arianna Rossetti · Alessandro Paciaroni · Barbara Rossi · Cettina Bottari · Lucia Comez · Silvia Corezzi · Lucio Melone · László Almásy · Carlo Punta · Andrea Fiorati

Received: 31 August 2022 / Accepted: 11 January 2023 / Published online: 22 January 2023

Abstract In the last years, hydrogels from renewable biopolymers and low-cost row materials are a hot topic for biomedical applications. In this context, cellulose nanofibrils are considered suitable building blocks for the synthesis of many biocompatible products, with a variety of chemical-physical properties. Herein we report a multi-technique and multi-scale study, from the molecular to the nanometric length scale, of the sol–gel transition observed in aqueous solutions of TEMPO-oxidized nano-sized cellulose fibrils (TOCNFs), when in the presence of polyvalent cations (Mg^{2+} and Ca^{2+}). We combine the data from Small Angle Neutron Scattering (SANS), which provide information about the inner structure of the nanofibril, with those from UV Resonant Raman (UVRR) spectroscopy, which is a sensitive probe of the intra- and inter-molecular interactions in the gel and the liquid state. The transition between the gel and the liquid phases is investigated as a function of the concentration of both TOCNFs and cations, the nature of the latter, and the pH at which the phenomenon is observed. SANS analysis reveals that ion concentration induces an anisotropic swelling in the nanofibrils which, at the same time, become more and more flexible. The nanofibrils flexibility is also dependent on TOCNF concentration and pH value. UVRR allows us to elucidate the structural organization and hydrogen-bonding properties of water in

Supplementary Information The online version contains supplementary material available at https://doi.org/10.1007/s10570-023-05058-2.

A. Rossetti · L. Melone · C. Punta · A. Fiorati (✉)
Department of Chemistry, Materials and Chemical Engineering "G. Natta", Politecnico di Milano, via Mancinelli 7, 20131 Milano, Italy
e-mail: andrea.fiorati@polimi.it

A. Rossetti · C. Punta · A. Fiorati
INSTM - Local Unit c/o Politecnico di Milano, via Mancinelli 7, 20131 Milano, Italy

A. Paciaroni · S. Corezzi
Department of Physics and Geology, University of Perugia, via A. Pascoli, 06123 Perugia, Italy

B. Rossi · C. Bottari
Elettra Sincrotrone Trieste, Strada Statale 14 Km 163.5, Area Science Park, 34149 Basovizza, Trieste, Italy

B. Rossi
Department of Physics, University of Trento, via Sommarive 14, 38123 Povo, Trento, Italy

L. Comez
Department of Physics and Geology, IOM-CNR c/o University of Perugia, via A. Pascoli, 06123 Perugia, Italy

L. Melone
Centro di Ricerca per l'energia, L'ambiente e Il territorio (CREAT), Università Telematica eCampus, Novedrate, Italy

L. Almásy
Institute for Energy Security and Environmental Safety, Centre for Energy Research, Konkoly-Thege Miklós út 29-33, 1121 Budapest, Hungary

aqueous TOCNF dispersions and gels, showing how water molecules partially lose their typical bulk-like tetrahedral organization when ions are added, and the gel phase is formed.

Graphical abstract

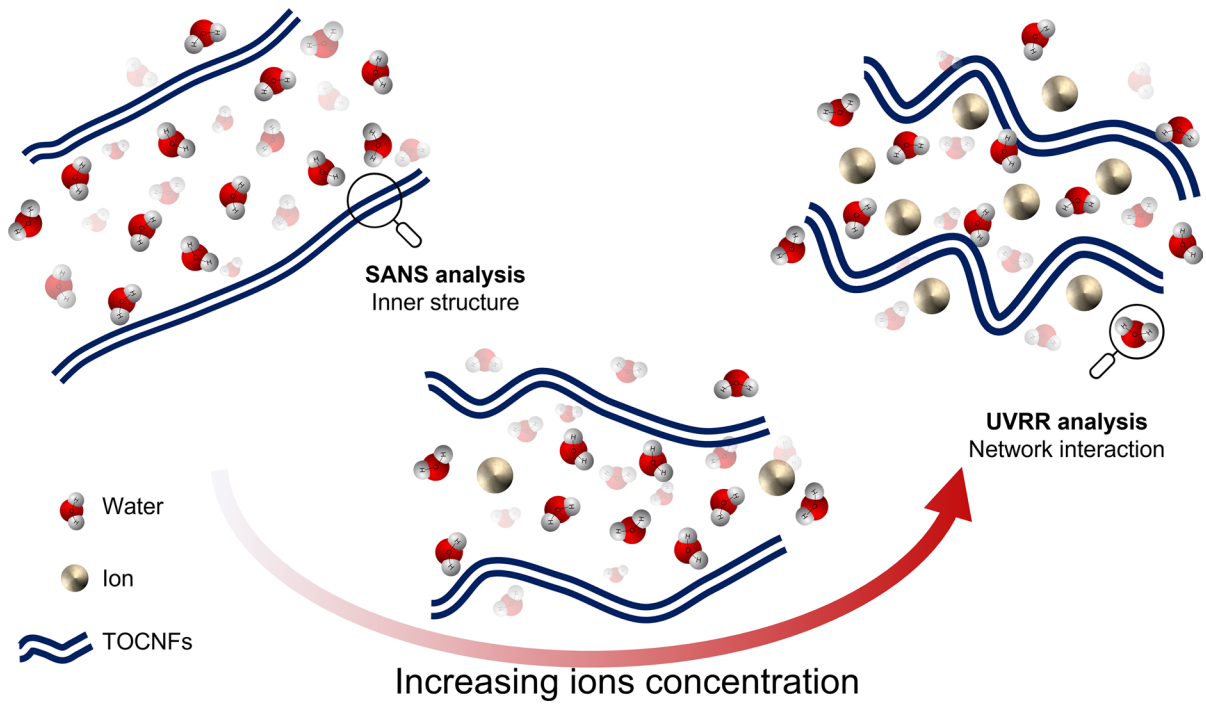

Keywords Cellulose nanofibrils · Cellulose-based hydrogels · SANS technique · UV Resonance Raman scattering technique · Inner nanostructure · Water interactions

Introduction

Hydrogels are considered particularly appealing materials for biomedical applications due to their high biocompatibility and the easy modulation of their chemical-physical properties, involving viscosity, stiffness, and degradation kinetics (Hoffman 2012). Moreover, their capability to carry drugs (Brannon-Peppas and Peppas 1989; Mauri et al. 2019), growth factors or cells, makes hydrogels a perfect class of materials already used in many branches of medicine, spanning from tissue engineering (Annabi et al. 2014) to injectable devices' production (Mauri et al. 2018; Vismara et al. 2020; Fiorati et al. 2020). Hydrogels are solid–liquid systems with three-dimensional cross-linked networks, formed by a variety of water-soluble polymers. It is possible to formulate gels with a wide range of chemical compositions, and in different forms, such as cylinders, nanoparticles, microparticles and films (Ullah et al. 2015).

Cellulose is a renewable biopolymer that can be obtained from biomass wastes, and which is naturally found mainly in plant cell walls with a hierarchical assembly of fibrils (Heinze et al. 2018). Cellulose in its different forms, including cellulose nanofibrils (CNFs), is of great importance to produce a wide range of bio-based materials for an uncountable applications. For sake of examples, cellulose, CNFs and their derivatives have been successfully employed in different fields: as hydrogels for biomedical applications (Bonetti et al. 2022; Zou et al. 2022), as modified drug release scaffolds (Celebi et al. 2016), as functional ingredients in food (Li 2002; Crawford et al. 2012; De France et al. 2017), in the formulation

of microbeads (Coombs OBrien et al. 2017), for preparing air-filtering systems (Lippi et al. 2022; Stanislas et al. 2022), and as a component in composite materials (Miao and Hamad 2013; Riva et al. 2021; Lan et al. 2022; Tanpichai et al. 2022).

The regioselective oxidation of the primary hydroxyls of cellulose to the corresponding carboxylic groups, catalysed by 2,2,6,6-tetramethylpiperidine 1-oxyl (TEMPO), furnishes a simple and widely used protocol for the surface modification of cellulose (Fig. 1) (Silva Perez et al. 2003; Saito and Isogai 2004; Pierre et al. 2017). Moreover, the introduction of negatively charged carboxylate groups at the C6 position of the glucopyranose rings opens the route to the preparation of nano-sized cellulose fibrils (TOCNFs, TEMPO-oxidized cellulose nanofibrils), by cleaving the hierarchical structure of the fibre, thanks to the electrostatic repulsion among single nano-fibrils (Isogai et al. 2011). TOCNFs possess a high surface charge (ζ-potential < -30 mV (Fukuzumi et al. 2014)) and a high aspect ratio, which means fibrils with up to a few µm in length and 5–10 nm in diameter (Habibi et al. 2006; Saito et al. 2011; Quennouz et al. 2016). Aqueous dispersions of TOCNFs exhibit interesting viscoelastic properties, going from low viscous solutions to highly viscous fluids and up to gels as a function of their concentration, even when the concentration is very low (0.2–0.3% w/w) (Pierre et al. 2017; Mendoza et al. 2018; Valencia et al. 2020). Moreover, TOCNF aqueous dispersions can switch reversibly from an elastic- to a viscous-dominated regime, a behaviour typical of thixotropic materials (Mendoza et al. 2018). Furthermore, the gelation process of TOCNF aqueous dispersions can be improved and tuned by varying different conditions, like pH (Saito et al. 2011), temperature, surfactants (Crawford et al. 2012; Quennouz et al. 2016), and electrolytes (Dong et al. 2013; Fukuzumi et al. 2014; Masruchin et al. 2019; Fiorati et al. 2020) concentration. Among all these approaches, the addition of polyvalent electrolytes (*e.g.* Ca^{2+}, Mg^{2+}) into TOCNF dispersions appears to be the most feasible synthetic approach, being able to promote the electrostatic cross-linking among fibrils (Geng et al. 2017;

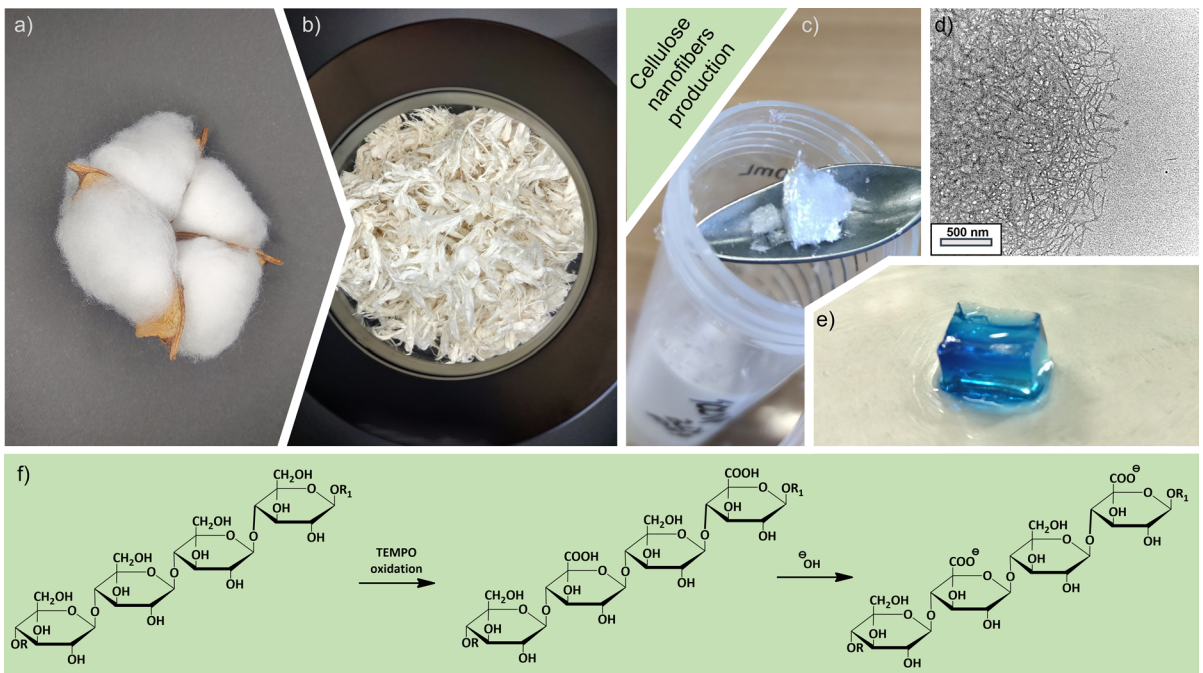

Fig. 1 Schematic representation of TOCNF hydrogels production from cotton boll to the final hydrogel: **a** representative picture of cotton boll, **b** macroscopical aspect of TEMPO-oxidised cellulose, **c** freeze-dried TEMPO-oxidized cellulose nanofibrils, **d** TEM image of TOCNF dispersion (2% w/w, scalebar 500 nm), **e** TOCNF hydrogel crosslinked (10 mM of Ca^{2+}, pH 7, coloured with indigo dye to improve the visualization), **f** Schematic representation of regioselective oxidation of the primary hydroxyls of cellulose to the corresponding carboxylic groups and its deprotonation

Mendoza et al. 2018; Diener et al. 2020). This leads to the reported capability of TOCNFs to form hydrogels with tuneable mechanical stability, suitable for different applications. Good cytocompatibility of these systems has been assessed in our recent studies and other literature (Hua et al. 2016; Rashad et al. 2017; Fiorati et al. 2020, 2021; Pitton et al. 2021).

Detailed structural information becomes crucial for the understanding of the role played by parameters like nanofibrils amount, ions concentration and pH in order to finely tune their properties before the loading of drugs or cells in biomedical applications. In this context, small-angle scattering techniques can offer direct information about the nanostructure of gel-like matter, often on multiple length scales, characteristic of complex systems with hierarchical morphology (Su et al. 2014; Geng et al. 2017; Mao et al. 2017; Guccini et al. 2018). Scattering studies on TOCNFs are already present in the literature, but experiments are usually reported on very low fibrils concentrations and neglecting the effect of ions, which are conditions far away from useful biomedical applications (Geng et al. 2017; Mao et al. 2017). In fact, Mendoza and co-workers have reported that CNF concentrations should be higher than 0.29% w/w in order to obtain solutions with a gel-like behaviour and proper thixotropic characteristics (Mendoza et al. 2018).

Here we report an in-deep investigation of the inner characteristics of TOCNF hydrogels as a function of nanofibrils and ions (Ca^{2+} and Mg^{2+}) concentrations, at three different pH values, by means of small-angle neutron scattering (SANS) and UV Resonant Raman scattering (UVRR) techniques. The joint combination of these two techniques allows us to probe the molecular properties of the systems and their microscopic structure on different length scales. SANS is exploited to provide a quantitative structural view of TOCNF hydrogels, by monitoring both topological changes and flexibility of nanofibrils at the nanometric length scale. From a molecular point of view, vibrational spectroscopies are widely used for investigating the chemical architecture and the distribution of functional groups in hydrogel materials. In particular, UVRR is a valid tool for retrieving information on the structural rearrangement of water molecules in TOCNF hydrogels. The hydrogen-bond dynamic of water is closely related to the confinement effects in the hydrogel nano-spaces and the presence of hydrophobic/hydrophilic groups at the TOCNF-solvent interface. Both these factors play an important role in determining the water swelling and gelation phenomena of the TOCNF hydrogels. The combination of the structural and molecular views offered by SANS and UVRR provides a comprehensive picture of the self-organization in TOCNF hydrogels under different conditions.

Materials and methods

Cellulose from cotton linters was kindly provided by Bartoli S.p.A. (Carraia (Lu), Italy). All chemicals were commercially available (Merck) and were used without further purification.

Cellulose oxidation

TEMPO-oxidized cellulose (TOC) was prepared as described in the literature (Isogai et al. 2011; Pierre et al. 2017). Briefly, 10 g of cotton linters were dispersed in deionized water (100 mL), then added to 200 mL of an aqueous solution containing KBr (1.54 g, 12.9 mmol) and TEMPO (0.215 mg, 1.38 mmol) and the final volume was adjusted to 570 mL by means of addition of water. A NaClO solution (12.5% w/w aqueous solution – 43.7 mL) was added dropwise in 2.5 h, and, in the following 4 h, the pH value was kept in the range 10–11 by adding NaOH (aq.) (4 M, about 25 mL). The reactive mixture was left under vigorous stirring overnight and then acidified to pH about 2 with aqueous HCl (37% w/w) obtaining the coagulation of cellulose. The white solid was filtered and washed with water (5 × 150 mL) and acetone (2 × 100 mL) obtaining 8.6 g of TOC (86% yield). The amount of carboxylic groups was determined through colourimetric titration with a NaOH solution and phenolphthalein as the indicator, resulting in 1.51 mmol g^{-1}. Ancillary information about the crystallinity index was obtained by means of XRD analysis resulting in a value of 64.4% (see details in SI S1 and Fig. S1).

Hydrogel preparation

In order to exploit the isotopic contrast between the solvent and the TOCNF network, each specimen intended for SANS experiments was prepared by using D_2O as the solvent for solutions and nanofibrils

dispersions. In addition, hydrogen–deuterium exchange of TOC hydroxyl moieties was previously promoted by means of repeated washing cycles in D_2O, in order to reduce the incoherent contribution to the measured total scattering cross sections. Generally, 1 g of TOC was suspended in 5 mL of D_2O and stirred for 1.5 h, then recovered by filtration; this process was repeated 5 times. After the last cycle, the samples were frozen at – 80 °C and freeze-dried until complete sublimation of the solvent.

Different stock dispersions of TOCNFs (1.12 or 2.25% w/v, pH 5, 7 and 11) were prepared by adding 0.45 g or 0.90 g of TOC in 35 mL of D_2O, followed by neutralization with a stoichiometric amount of NaOD (1 equivalent with respect to the content of carboxylic groups). Then the mixture was sonicated (Branson Sonifier 250, 13 mm probe tip working at 20 kHz in pulsed mode) at 0 °C until a colourless and transparent viscous dispersion was obtained. Finally, the pH was set to 7, 5 or 11 by the addition of DCl or NaOD in D_2O (0.01 M) and the volume was adjusted to 40 mL with deuterium oxide.

TOCNF hydrogels were prepared by adding precise amounts of D_2O and ions solutions ($CaCl_2$ or $MgCl_2$, 100 or 150 mM in D_2O) to the proper stock dispersion in order to reach the desired final concentration (Table 1). For rheological and UVRR investigations, the gels were prepared in H_2O and the isotopic exchange was avoided. Prior to analysing the samples, the gels were left to reticulate for at least 15 min at room temperature.

Transmission electron microscopy (TEM)

TOCNF samples (0.25%, pH 7) for transmission electron microscopy (TEM) analysis were prepared by depositing a drop of TOCNF dispersion on a 3 mm 200 mesh copper grid coated with a thin layer of amorphous carbon and letting it air-dry overnight at room temperature before analysis. All grids were observed under a Philips CM 200 field emission gun (FEG) TEM operating at an accelerating voltage of 200 kV. The width of a representative bunch of 395 fibrils was measured by means of ImageJ software (Schneider et al. 2012).

Table 1 List of tested TOCNF hydrogel samples

TOCNF concentration [%]	pH	$CaCl_2$ [mM]	$MgCl_2$ [mM]
1	7	0	0
1	7	1	0
1	7	2	0
1	7	5	0
1	7	7	0
1	7	10	0
1	7	15	0
1	7	0	1
1	7	0	2
1	7	0	5
1	7	0	7
1	7	0	10
1	7	0	15
2	5	0	0
2	5	10	0
2	11	0	0
2	11	10	0
2	7	0	0
2	7	1	0
2	7	2	0
2	7	5	0
2	7	7	0
2	7	10	0
2	7	15	0
2	7	0	1
2	7	0	2
2	7	0	5
2	7	0	7
2	7	0	10
2	7	0	15

Rheology

Rheological measurements were conducted by means of an AR2000 rotational rheometer (TA Instrument, New Castle, DE, USA) equipped with cone-plate geometry (D = 40 mm, angle = 1°, polyacrylic material). A solvent trap accessory was employed to avoid solvent evaporation. The specimen temperature was set at 20 °C by means of a Peltier plate. The shear rate sweep range was from 0.1 to 1000 s^{-1}.

SANS measurements

SANS measurements were performed on the diffractometer Yellow Submarine (BNC, Budapest) in the wavevector Q-range from 0.007 to 0.3 $Å^{-1}$ (Almásy 2021). The instrument setup consisted of a mechanical velocity selector providing a wavelength resolution of 0.2 FWHM, and a BF_3 gas-filled area detector with 1×1 cm^2 pixel size. The samples were contained in Hellma quartz cells of 5 mm light path and were thermostated at 25 °C. Standard data corrections were performed by the BerSANS software package (Keiderling 2002).

SANS data fitting

To obtain quantitative information from the SANS data we applied a model able to describe the measured scattered intensity in the whole accessible Q range, while being sound to represent the topology properties of TOCNFs. The TOCNFs are described as a worm-like chain with a rectangular cross-section (Pedersen and Schurtenberger 1996), whose corresponding static structure factor, not including excluded-volume effects, reads as follows:

$$S(Q) = S_{chain}(Q)S_{cs}(Q) \tag{1}$$

The first factor represents the contribution from a flexible chain of contour length L, consisting of statistical segments with a Kuhn length b that quantifies the local stiffness of the chain. As such, $S_{chain}(Q)$ follows the Debye-like Q^{-2} behaviour at a Q value before crossing over to a Q^{-1} dependence, which is the characteristic signature of rigid linear structures (Zemb and Lindner 2002). An analytic expression in the whole Q range, obtained by fitting Monte Carlo data of semiflexible chains, is given by (Pedersen and Schurtenberger 1996):

$$S_{chain}(Q) = S_{SB}(Q)\chi(Q) + S_{loc}(Q)(1 - \chi(Q)]) \tag{2}$$

where

$$S_{SB}(Q) = S_{Debye}(Q) + \left[4 + \frac{7}{Q^2R_g^2} - \left(11 + \frac{7}{Q^2R_g^2}\right)e^{-Q^2R_g^2}\right]\frac{b}{15L} \tag{3}$$

with $R_g^2 = Lb/6$ and

$$S_{Debye}(Q) = \frac{2\left[e^{-Q^2R_g^2} + Q^2R_g^2 - 1\right]}{(Q^2R_g^2)^2} \tag{4}$$

and

$$S_{loc}(Q) = \frac{1}{LbQ^2} + \frac{\pi}{LQ} \tag{5}$$

In Eq. (3), $S_{SB}(Q)$ is the Sharp-Bloomfield expression, that here describes the low-Q contribution of a semi-flexible chain (Sharp and Bloomfield 1968) and smoothly tends to the local rod-like behaviour given by $S_{loc}(Q)$ through the interpolating function $\chi(Q) = exp[\left(-(Qb)/q_1\right)^{p_1}]$, where $q_1 = 5.53$ and $p_1 = 5.33$.

Finally, the Q^{-4} Porod range in the high-Q region of Eq. 1 is described through a rectangular cross-section, consistent with the model for TOCNF units proposed by Mao et al. (Mao et al. 2017) given by:

$$S_{cs(Q)} = \pi L\left(a_1a_2\right)^2 exp\left[-\frac{Q^2}{8\beta}\left(a_1^2 + a_2^2\right)\right]I_0\left[\frac{Q^2}{8\beta}\left(a_2^2 - a_1^2\right)\right] \tag{6}$$

where $I_0[x]$ is the modified Bessel function of the first kind of zeroth order, β is a constant equal to 2.59, a_1 and a_2 are the side dimensions of the rectangular cross-section.

UV Resonance Raman scattering

UVRR experiments were carried out exploiting the setup available at the BL10.2-IUVS beamline of Elettra Sincrotrone Trieste (Italy) as described elsewhere (Rossi et al. 2020). UVRR vertical–vertical polarized spectra of TOCNF hydrogels were collected using 266 nm as excitation wavelength and acquired in back-scattering geometry by using a triple-stage spectrometer (Trivista, Princeton Instruments) with a spectral resolution of about 4 cm^{-1}. The experimental setup was standardized by measuring the depolarization ratio of symmetric and antisymmetric modes of CCl_4. The final radiation power on the samples was kept at about 0.4 mW. Any possible photochemical decomposition due to prolonged exposure to UV radiation was avoided by means of a slow oscillation of the sample cell during the measurements in order to continuously change the illuminated volume.

The OH stretching band of water observed between 2800 and 3800 cm^{-1} in the UVRR spectra of TOCNF hydrogels was reproduced by considering three distinct components: a mixed Gaussian–Lorentzian form for the lowest-wavenumber component ($w1$=3200 cm^{-1}) and two Gaussian profiles for the two other contributions ($w2$=3450 and $w3$=3600 cm^{-1}). In the fitting procedure, the widths of the three components were kept fixed. Even if various decomposition procedures have been proposed to describe the OH band features, here we employed a relatively simple scheme that uses the minimum number of components needed to reproduce the band profile. This method, which involves a reduced number of parameters, has proved to be convenient for comparison purposes.

Results and discussion

Oxidation of cellulose and TEM microscopy

The TEMPO oxidation approach is widely reported to produce cellulose nanofibrils with a high aspect ratio. In particular, the obtained nanofibrils are generally described as parallelepipeds possessing cross-sectional dimensions in the nanometric scale (a_1=2–4 nm, a_2=7–10 nm) and lengths in the micron-scale Fig. 2a (Saito and Isogai 2004; Isogai et al. 2011; Geng et al. 2017; Mao et al. 2017; Pierre et al. 2017).

As a consequence of this oxidation, the carboxylic moieties on the surface of the nanofibrils can be exploited to induce strong electrostatic repulsions between the strands, affording stable colloidal suspensions. Cellulose from cotton linters was successfully oxidized obtaining a carboxylic content of

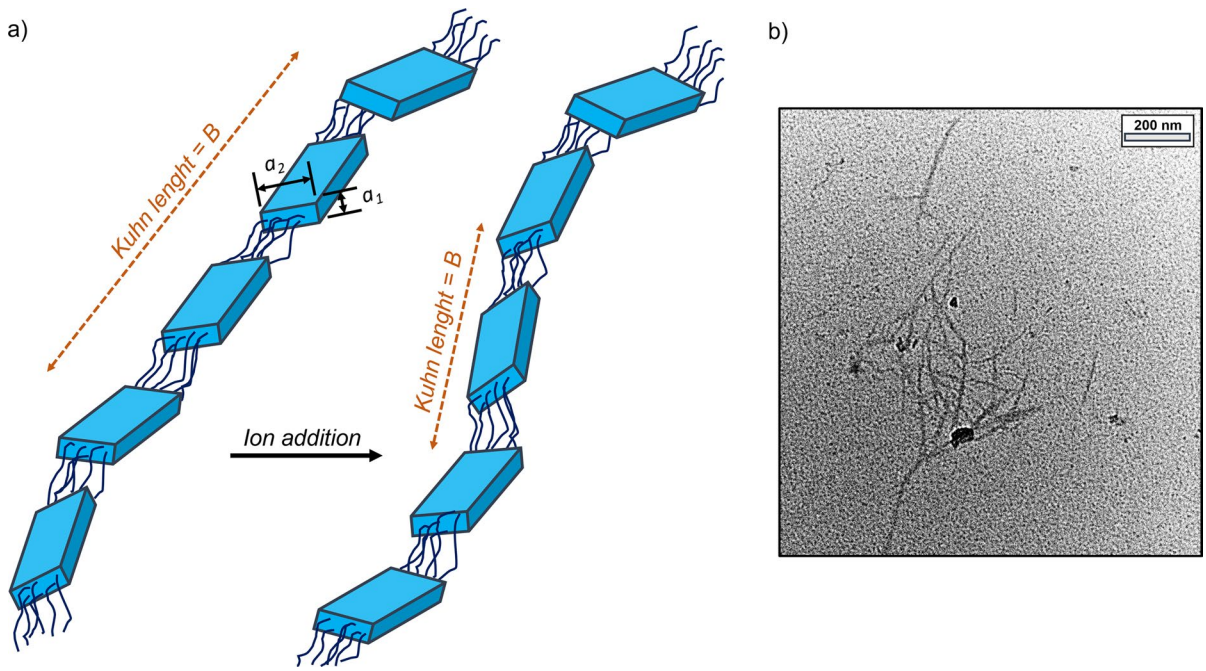

Fig. 2 **a** Schematic representation of a TOCNF: the parallelepipeds represent the crystalline regions whereas the lines are intended as the cellulose chains in the amorphous region. The addition of polyvalent ions induces a fibril bending resulting in a decrease of the Kuhn length measured by SANS analysis. **b** TEM image of the TOCNF dispersions (0.25%, pH 7) used as the stock solution, scalebar 200 nm

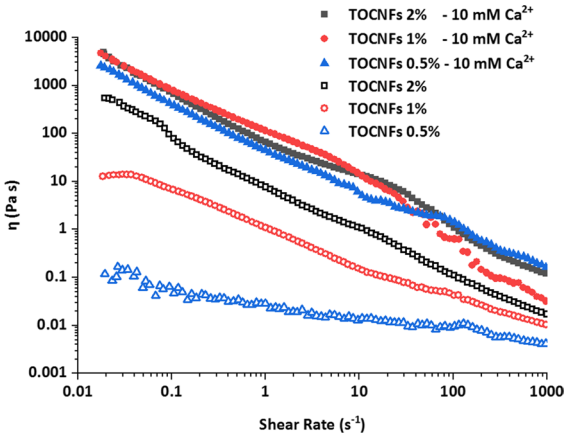

Fig. 3 Shear viscosity *vs* shear rate for TOCNF dispersions as a function of nanofibrils and ions concentration

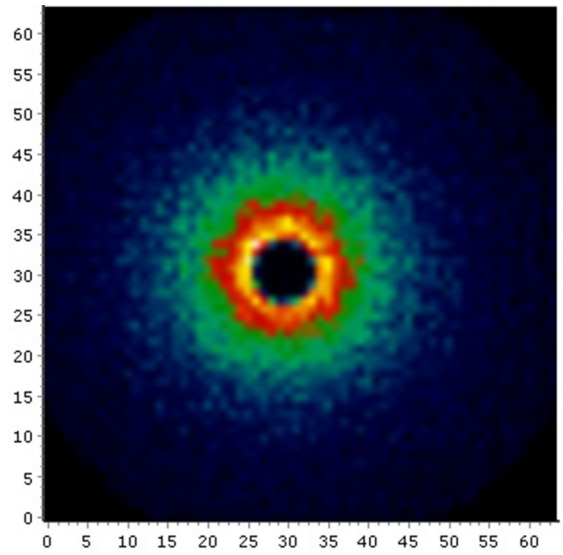

Fig. 4 2D SANS scattering profile of TOCNF dispersion (2%, pH 7, 0 mM Ca^{2+})

1.51 mmol g^{-1}. From a dimensional point of view, the obtained nanofibrils possess a mean width of 8.2 nm (about 90% of them are in the 5–10 nm range), and a length between 250 and 800 nm, as observed by TEM microscopy (Fig. 2b, and Fig. S2), in good accordance with the literature. A quantitative assessment of the cross-sectional dimensions of these TOCNFs was carried out by means of SANS, as described later in the manuscript.

Rheology

Before analysing the structure at a molecular level, gelation experiments were performed to get an idea of how the systems behave at a macroscale level. In Fig. 3 we show the steady-state shear viscosity versus the shear rate of three different TOCNF aqueous dispersions (0.5, 1.0 and 2.0% w/w), in the absence (unfilled markers) or presence (filled markers) of Ca^{2+} ions (10 mM). In order to mimic biomedical application conditions, the pH of all the dispersions was corrected to 7 by means of dropwise addition of NaOH (0.01 M) or HCl (0.01 M). The results achieved for dispersions containing 0.5% w/w of TOCNFs are in good agreement with the data reported by Geng and co-workers (Geng et al. 2017) but, as expected, the increase in viscosity is much greater when the gelation is induced by Ca^{2+} ions. The bumpy trends of flow curves suggest the presence of some inhomogeneities in the gelation transition. The achieved results are in good agreement with the literature, however, in-depth rheological characterization is outside the scope of this work as it was already reported elsewhere (Dong et al. 2013; Geng et al. 2017; Mendoza et al. 2018; Aaen et al. 2019).

It is widely recognized that the rheological behaviour of TOCNF dispersions is strictly dependent on parameters like nanofibrils concentration and ionic strength. Indeed, Geng and co-workers report that dispersions of TOCNFs obtained from jute (oxidized at about 1.5 mmol g^{-1}) behave like Newtonian fluids when the concentration is below 0.1% and show a shear thinning behaviour at higher concentrations. A sharp viscosity transition is also observed at a concentration of about 0.2% (Geng et al. 2017). In the same work, the authors deeply investigate, by means of rheology and small-angle X-Ray scattering, the sol–gel transition of the system induced by shielding the TOCNF superficial charges using different concentrations of NaCl. Despite the interesting results reported, the investigated hydrogels do not possess the rheological properties and the stiffness generally required for some of the biomedical applications mentioned in the introduction section. For these practical reasons, many authors generally prefer to use higher cellulose concentrations (up to 2% w/w) and to induce the gelation process by using polyvalent cations like Ca^{2+}, Mg^{2+} or Fe^{3+}. In these cases, the rheological properties are strongly dependent on the

valency of the ions and their binding strength with carboxylate groups of TOCNFs (Dong et al. 2013).

Structural information from SANS data analysis

Structural information at the nanometric scale on TOCNF dispersions and relative ion-induced gelation processes were achieved by means of the analysis of SANS data. The effect of ions concentrations was explored in the 0–15 mM range, by adding different amounts of Ca^{2+} or Mg^{2+} solutions to two stocks of TOCNF dispersions (1% and 2% w/w) at different pH values. The detailed list of samples is reported in Table 1.

As an example, in Fig. 4 we report the 2D scattering profile of TOCNF 2% dispersions, measured at a sample-detector distance of 5.125 m, and using an incident wavelength of 4.4 Å. All the observed profiles indicate that the samples are isotropic over the entire Q-range.

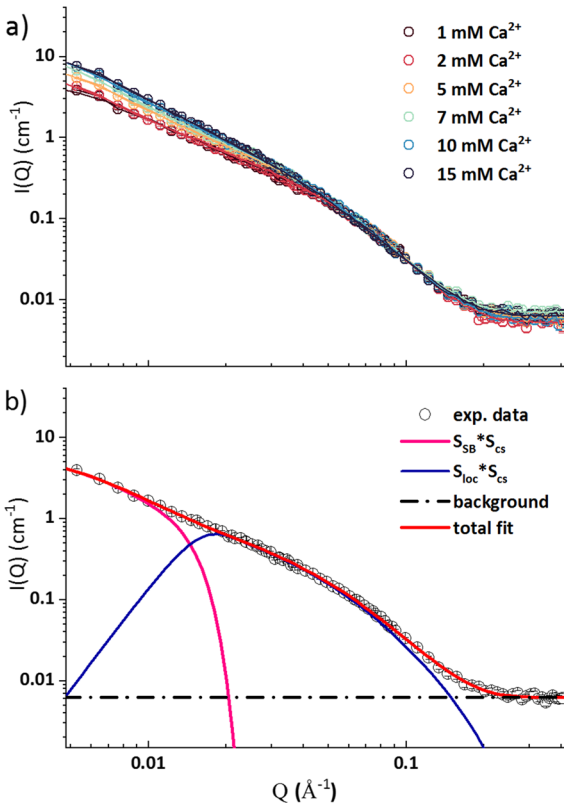

Fig. 5 **a** Scattering intensity $I(Q)$ as a function of the scattering wavevector amplitude Q for the samples of 1% TOCNF hydrogels at pH = 7 and several Ca^{2+} concentrations (open symbols: experimental data, continuous lines: fitting curve, see Eq. 2 in the text). **b** Example of best fitting for the samples of 1% TOCNF hydrogels at pH = 7, 0 mM Ca^{2+}

Figure 5a shows the typical scattering intensity $I(Q)$ as a function of the wavevector Q, measured for the gel samples of TOCNF 1% dispersions at different concentrations of ions.

As previously mentioned (Materials and Methods. Hydrogels Preparation), D_2O was used in the place of H_2O to prepare all the samples in order to maximize the contrast between solvent and nanocellulose components. In more detail, the significant difference between the scattering length density of D_2O and nanocellulose, respectively 6.34 10^{-6} $Å^{-2}$ and 1.77 10^{-6} $Å^{-2}$, allowed us to straightforwardly single out the SANS signal from the macromolecules. At the same time, using a deuterated solvent was functional to reduce the incoherent background, thus improving the signal/noise ratio. All the experimental profiles show, as dominant features, an upturn at low Q-values and a broad shoulder in the medium Q-range between 0.01 and 0.1 $Å^{-1}$. In the literature, the 1D scattering profiles of diluted TOCNF dispersions are generally modelled with form factors like parallelepiped (Geng et al. 2017) or ribbon models with rounded edges (Su et al. 2014; Mao et al. 2017). Despite a Gaussian-approximated parallelepiped model well describes the intensity profiles in the Q range 0.03–0.3 $Å^{-1}$, this mathematical approach does not fit properly the lower Q region of the spectra. This was attributed to the flexibility of TOCNF chains, which may be affected by both the ions and nanocellulose concentration and pH. The experimental data are excellently fitted by Eq. 1, as shown in Fig. 5 for the samples containing TOCNFs 1% and pH = 7, as a function of Ca^{2+} concentration. A similar quality of the fit was obtained for all the samples (Fig. S3). The proposed model combines the flexible ellipsoidal cylinder model, reported by Courtenay and co-workers for cationic cellulose nanofibril hydrogel (Courtenay et al. 2018), and the parallelepipedal form factor models, described above (Geng et al. 2017). This flexible parallelepipedal model describes the "TOCNFs as chains constituted" by effective rigid segments freely connected with each other.

The structural parameters corresponding to the TOCNF unit determined through Eq. 1 from the SANS data are a_1, a_2, b, and the contour length L.

The parallelepiped dimensions are described by a_1, a_2, and L (Fig. 2a), whereas b describes the Kuhn length. The parameter b is representative of the length of the rigid segments composing the nanofibrils and is used to depict the stiffness of the TOCNFs forming the hydrogels, according to the literature (Courtenay et al. 2018).

The contour length L is too large to be safely estimated in the accessible experimental Q range. In detail, the lengths of the prepared TOCNFs are on the micron scale, as confirmed by TEM micrography (Fig. 2b), and in accordance with the literature, they would provide a SANS signal in the Q-range below 0.007 $Å^{-1}$ (Gu and Mildner 2016).

Concerning the parallelepiped cross-sectional dimensions (a_1 and a_2 in Fig. 2a) the values estimated by the fitting procedure are in good agreement with the data reported in the literature (Habibi et al. 2006; Saito et al. 2011; Quennouz et al. 2016). In particular, the shorter cross-sectional dimension (the height a_1 in Fig. 2a) seems to be independent from ion concentration and turns out to be 22 ± 1 Å and 23 ± 1 Å, respectively, in the case of TOCNFs 1% and TOCNFs 2% at all the investigated Ca^{2+} concentrations.

Similar values are obtained by crosslinking the TOCNFs with Mg^{2+}, being a_1 equal to 21 ± 1 Å for TOCNFs 1% and 22 ± 1 Å for TOCNFs 2% (Fig. 6a).

On the contrary, the larger cross-sectional dimension (the width a_2 in Fig. 2a) is found to be dependent

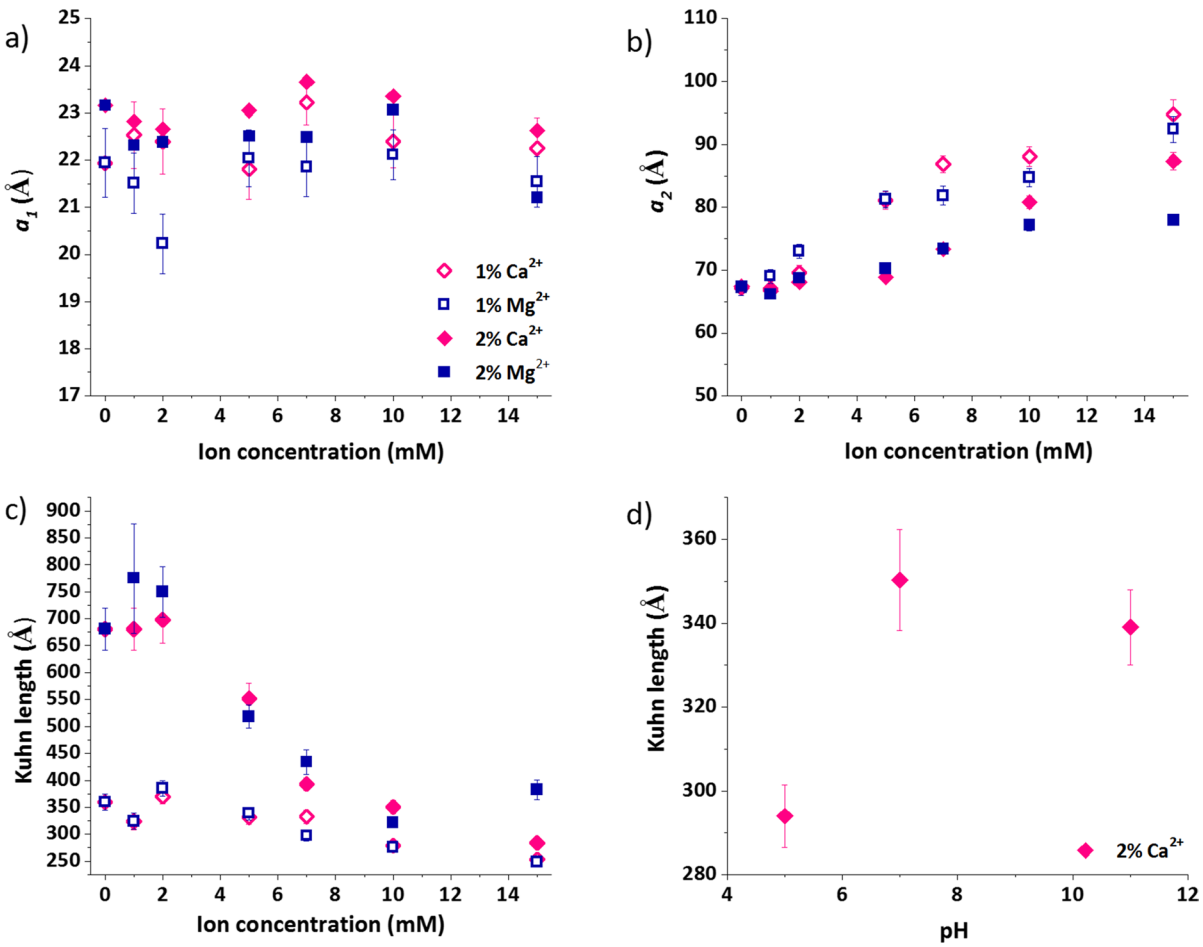

Fig. 6 Dependence on ions concentration of the cross-sectional dimensions a_1 (**a**) and a_2 (**b**) for the samples of TOCNF hydrogels at 1 and 2% of cellulose (empty and filled symbols, respectively) at pH = 7 with either Ca^{2+} or Mg^{2+}. Dependence of the Kuhn length on ions concentration (**c**) and pH (**d**)

on the ion concentration, being constant at lower values, but increasing when the ions overcome a certain threshold value. In particular, in the case of TOCNFs 1%, for both Ca^{2+} and Mg^{2+}, a_2 seems to be stable at around 67 ± 2 Å up to the 2 mM ion concentration, and then increases with the ion concentration to attain a value of about 90 Å (Fig. 6b).

These results indicate a significant anisotropic swelling of the cellulose nanofibrils, which occurs after reaching an ion threshold value. In the case of TOCNFs 2%, analogous results are obtained, but the onset of the observed swelling effect is shifted to a higher ion concentration of about 5 mM, and its extent is significantly lower, with a_2 increasing toward a plateau value of about 80 Å (Fig. 6b). This suggests that, when the TOCNF concentration raises, the electrostatic repulsion begins to be effective, thus limiting the fibrils swelling. The need for about a double ion concentration to produce similar effects when using TOCNFs 2% instead of 1% is expected because a double amount of carboxylic moieties has to be coordinated by the cations. In addition, no significant differences can be observed between the two investigated species (Ca^{2+} and Mg^{2+}).

As for the dependence of the Kuhn length as a function of cation concentration and pH we find the behaviour shown in Fig. 6c and d. Irrespective of the kind of ion, for TOCNFs 1% there is only a slight decrease of b above 6 mM from 350 ± 20 Å to 270 ± 20 Å. On the other hand, for TOCNFs 2% the Kuhn length undergoes a remarkable reduction above approximately 2 mM from 740 ± 40 Å down to 340 ± 40 Å, attaining similar values as in TOCNF 1% samples (Fig. 6c). These results suggest that by increasing ion concentration the system becomes progressively more flexible, in accordance with the literature (Courtenay et al. 2018). This is consistent with a picture where a high cation content can effectively screen the electrostatic repulsion forces among nanocellulose fibrils acting as a cross-linking agent for the carboxylates moieties.

In the case of TOCNFs 2%, it is possible to suppose that the nanofibrils arrange themselves as linearly as possible, minimizing the repulsion between the negative charges. The ions addition firstly induces cross-link among different fibrils, resulting in no Kuhn length variation. Then, the increase of ions concentration leads to bending of the fibrils due to intramolecular cross-linking, which means between carboxylates placed on the same fibril. This effect is less evident when the TOCNF concentration is low (1%) because the fibrils have more space to arrange themselves, leading to a more flexible conformation.

The effect of the electrostatic repulsion is further confirmed by the significant variation of the Kuhn length found when the pH is changed (Fig. 6d). Indeed, the acidic samples, where the carboxylic moieties are uncharged, are much more flexible than the basic ones which possess negative surface charges. To note, that both parallelepiped cross-sectional dimensions do not change appreciably with pH, with $a_1 = 22 \pm 1$ Å and $a_2 = 68 \pm 2$ Å.

In a recent work, Valencia and co-workers have observed a multivalent ion-induced re-entrant transition on 0.2–0.1% w/w TOCNF dispersions (Valencia et al. 2020), *i.e.* a swelled-to-collapse-to-swelled state which can be seen and theoretically predicted on polyelectrolyte nanogels (Jha et al. 2012; Sing et al. 2013). Interestingly, from SAXS experiments and molecular dynamics simulations they evaluated different swelling states of the nanofibrils as a function of ions concentration. In detail, a swollen state was detected at 1 mM concentration of Zn^{2+}, which collapsed when the Zn^{2+} concentration was increased to 2 mM and then swollen again when the concentration further increased to 3 mM (Valencia et al. 2020). By measuring the rheological properties of the obtained hydrogels, they observed an increase in the gel storage modulus (G') until a critical salt concentration was reached, while further addition of metal ions led to its decrease. However, this latter effect does not clearly appear in the work reported by Aaen and co-worker (Aaen et al. 2019), suggesting that in-depth studies of rheological properties as a function of swelled-collapsed TOCNF state may be needed to clarify some aspects.

As in other cases reported in literature (Su et al. 2014; Geng et al. 2017; Mao et al. 2017; Valencia et al. 2020), these results were achieved using TOCNF concentrations too far from the biomedical application conditions (Dong et al. 2013; Fiorati et al. 2020), and without controlling the pH of the final hydrogels, which is an important parameter to be regulated when dealing with cells and organisms. Aiming at these conditions, especially looking for pH close to 7 and TOCNF concentration equal to 1–2%, we were able to observe that an anisotropic dimensional shrinking can be measured when Ca^{2+} is added to the sample,

in good agreement with the observation of Valencia and co-workers (Valencia et al. 2020).

UVRR: H-bond network of water in TOCNF hydrogels

Raman spectroscopy and in particular UVRR experiments can be a useful tool for providing details on the H-bond state of water molecules inside hydrogels' phases (Rossi et al. 2015b, a, 2018; Bottari et al. 2017). In particular, the Raman signal associated with the OH stretching band of water located in the 3000–3800 cm^{-1} wavenumber range can be used as a sensitive probe of the H-bond organization of water, as demonstrated in previous works (Maeda and Kitano 1995; Ratajska-Gadomska and Gadomski 2004; Joachimiak et al. 2005; Pastorczak et al. 2009). The use of UV wavelengths for exciting the Raman spectra has the further advantage of strongly reducing the interfering fluorescence background typically affecting the visible Raman spectra of hydrogel systems, thus simplifying the analysis of the vibrational profile.

Figure 7 displays the UVRR spectra acquired in the range 2850–3950 cm^{-1} for the samples of 2% TOCNF hydrogels with 0 and 10 mM Ca^{2+}. The spectra were normalized to their maximum intensity for a better comparison. It is noteworthy that the characteristic Raman profile of the OH stretching band of water dominates the vibrational spectra of TOCNF hydrogels in the investigated wavenumber region.

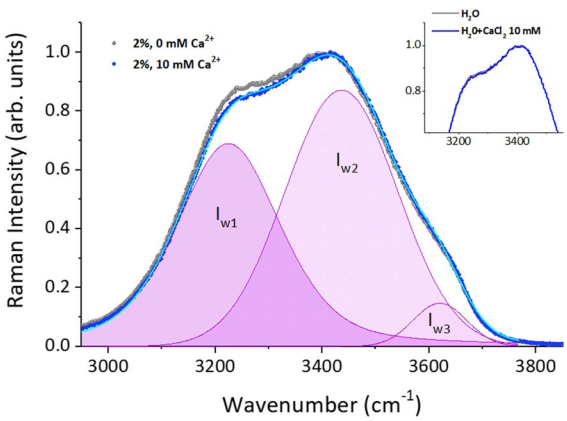

Fig. 7 Polarized UV Raman intensity for the samples of TOCNF hydrogels at 2% of cellulose with 0 and 10 mM of Ca^{2+} at room temperature in the spectral range 2850–3950 cm^{-1}. The spectra are normalized to their maximum intensity. Results of the fitting procedure for the sample at 10 mM of Ca^{2+} are reported in the same panel, as an example. The total fit-curve and the OH stretching components of water are represented with full cyan line and shaded areas, respectively. Inset: comparison between the UV Raman spectra collected for pure H_2O and the aqueous solution of Ca^{2+} at 10 mM in the spectral range 2850–3950 cm^{-1}

This Raman signal shows the presence of three distinct components centred at $w1$ = 3200, $w2$ = 3450 and $w3$ = 3600 cm^{-1}, typical of water. Following a common interpretation (Walrafen 1967; Green et al. 1986; Maeda and Kitano 1995; Eaves et al. 2005; Bottari et al. 2018), the component at the lowest wavenumber $w1$ can be associated with the collective in-phase vibrations due to water molecules locally arranged in ordered ice-like tetrahedral configurations (Walrafen 1967; Green et al. 1986), whereas the contribution at $w2$ is ascribed to water structures where H-bonds are partially elongated and/or distorted (Walrafen 1967) and phase correlations among nearest oscillators vanish. Finally, the shoulder at the higher wavenumber $w3$ is attributed to OH groups of water not involved as proton donors in H-bonds.

The spectra in Fig. 7 evidence a clear difference between the shape of the OH stretching band observed in samples of TOCNFs with and without the addition of ions. In particular, the vibrational profiles indicate a clear decrease of the ice-like component of water for the cellulose gels with 10 mM of Ca^{2+} with respect to the pure TOCNF dispersion. This finding suggests that the intermolecular structure of water in the compartmentalized spaces of the TOCNF hydrogel network is different from that found in the dispersion of cellulose, consistently with what has already been observed in other gel systems (Maeda and Kitano 1995; Ratajska-Gadomska and Gadomski 2004; Joachimiak et al. 2005; Pastorczak et al. 2009). We can argue that, when ions are added and the gel is formed, water molecules hydrating the cellulose fibrils partially lose their tetrahedral organization typical of the bulk. It is noteworthy that this effect observed on the local rearrangement of the water H-bonding network is exclusively attributed to the interaction of solvent molecules with the groups of TOCNF fibrils in the different gel states and not to the change in Ca^{2+} concentration. This is confirmed by the comparison between the UV Raman spectra collected for pure H_2O and the aqueous solution of Ca^{2+} at 10 mM in the spectral range 2850–3950 cm^{-1} (inset of Fig. 7) which does not evidence any detectable

change in the spectral shape of the OH stretching band of water induced by the addition of Ca^{2+} ions.

These spectral changes can be quantified by a curve-fitting procedure (Marinov et al. 2001; Sassi et al. 2004; Di Michele et al. 2006; Paolantoni et al. 2009; Bottari et al. 2018) as described in the section Materials and Methods, which allows us to distinguish the different spectral components of the OH stretching signal of water. An example of decomposition of the Raman profile for the sample of TOCNFs at 10 mM of Ca^{2+} is displayed in Fig. 7, the other deconvolutions are reported in Fig. S4.

In order to quantify the spectral changes described above, we have estimated the quantity $C = I_{w1}/I_{OHtot}$ where I_{w1} is the area of the lowest frequency component and $I_{OHtot} = I_{w1} + I_{w2} + I_{w3}$ is the sum of the areas I_{w1}, I_{w2} and I_{w3} of all the spectral contributions to the OH-stretching profile. The quantity C is related to the fraction of OH groups involved in ordered ice-like configurations (Rossi et al. 2018).

As reported in Fig. 8, the parameter C is dependent on the type and concentration of ions used in TOCNF hydrogels. In particular, the figure points out that the value of C tends to decrease significantly for concentrations of Ca^{2+} above 3–4 mM. Moreover, it is worth noting that the value of C estimated for TOCNF hydrogels is lower than that of the solvent at the same concentration of Ca^{2+}, suggesting that the interactions with the groups of cellulose fibrils affect the tetrahedral ordering of a large fraction of water molecules present into the gel matrix. It might be expected that the formation of H-bonds between water and hydroxyl groups on the surface of nanofibrils would play an important role in the destructuring of the ice-like configurations typical of bulk water. Interestingly, this destructuring effect on water entrapped in the TOCNF gel phase becomes remarkable starting from Ca^{2+} ions concentration of about 5 mM and endures up to the highest ions concentration examined. This suggests the formation of stronger H-bonds (HBs) between water molecules and groups of TOCNF fibrils induced by the addition of a larger amount of ions. As a matter of fact, the decrease of the parameter C due to the sol–gel transition is associated with a concomitant decrease of the Kuhn length (Fig. S5a), once a threshold concentration is overcome, suggesting that, consistently with SANS results, the fibrils bending induced by gelation could favour an H-bonding trading between water-water and ion mediated intramolecular H_2O-TOCNF interaction. A similar observation can be made by correlating the parameter C with a_2 (Fig. S5b): below a threshold concentration (placed in the range 2–5 mM) the values of a_2 and C are almost constant, once this threshold was overcome (> 5 mM), both parameters results affected.

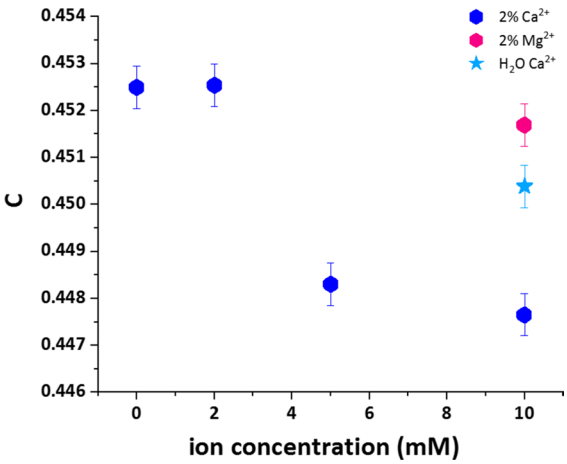

Fig. 8 Dependence on ions concentration of parameter C (estimated as described in the text) for the samples of TOCNF hydrogels at 2% of cellulose, pH = 7 and various types of ions (Ca^{2+} and Mg^{2+}). The star point represents the value of C obtained for the solvent used for hydrating cellulose

Additionally, we can observe from Fig. 8 that, in the case of TOCNF hydrogel obtained with the highest concentration of Mg^{2+} ions, the parameter C assumes values comparable to that of the solvent. This finding gives evidence that, in the TOCNF/Mg^{2+} gels, the formation of HBs between the nanofibrils and water molecules results like those formed in the solvent, leading to minor changes in their spectral distribution. Overall, these results from the UVRR study appear to be consistent with the observed increase in viscosity of TOCNF systems when the gelation is induced by Ca^{2+} ions, as detected by the rheology measurements. Moreover, as a remarkable result, we found that a progressive disruption of the tetrahedral order of water is strongly dependent on the valency and concentration of the ions that probably lead to different binding strengths between the TOCNF carboxylate groups and the solvent molecules.

Conclusions

In summary, in this work we reported a multi-technique and multi-scale approach aimed to observe the effect of the sol–gel transition induced by polyvalent cations (Mg^{2+} and Ca^{2+}) on TEMPO-oxidized nanodimensioned cellulose fibrils. The nanometric scale was investigated by means of SANS experiments, which provide detailed structural information about the nanofibril's behaviour as a function of ions concentration, and consequent cross-linking between the nanofibrils. At the same time, the properties of this system at a smaller (Ångström) scale were provided by studying the interaction between the solvent molecules (water) and TOCNFs.

From the analysis of SANS measurements, we were able to detect an anisotropic swelling in the nanofibrils, from 67 ± 2 Å up to about 90 Å. In addition, exploiting the information given by the Kuhn length parameter, we observed that when the concentration of nanofibrils is higher (2% w/w) these are more outstretched, to minimize the electrostatic repulsions. On the other hand, by decreasing the TOCNF concentration (1% w/w) the nanofibrils showed a smaller Kuhn length (350 ± 20 Å) even in absence of ions. The addition of ions (2 mM) for inducing the sol–gel transition strongly reduced the Kuhn length (from 740 ± 40 Å to 340 ± 40 Å) suggesting an intensified entanglement in the polymeric network. The higher the cation concentration used, the shorter the Kuhn length we found, whose value reached 270 ± 20 Å when the amount of ions was about 6 mM. In addition, it was observed that the carboxylates protonation, obtained by lowering the value of pH, further reduced the Kuhn length, therefore increasing the entanglement of the fibrils.

Since the UVRR spectra were dominated by the water signal, we were able to elucidate changes in the structure and the H-bonding properties of water in TOCNF dispersions and hydrogels. In particular, we observed that the water molecules partially lost their typical bulk-like tetrahedral organization when ions were added and the sol–gel transition occurred. This so-called destructuring effect on water can be ascribed to the formation of stronger H-bonds between the water molecules and the groups of CNF fibrils. A quantification of destructing effect as a function of concentration and valency of ions was provided by estimation of the parameter C. Interestingly, no appreciable modifications are detected for gelation induced by Mg^{2+} ions up to relatively high concentrations, whereas a progressive disruption of the tetrahedral order of water is observed when a larger amount of Ca^{2+} ions is added to TOCNF fibrils.

In conclusion, we observed that cation-induced sol–gel transition of TOCNF dispersions is associated with relevant changes at all the investigated scales. Indeed, it is related to a general increase of nanofibrils bending (hundred nanometres scale), which occurs contemporary to a swelling of the nanofibril itself (ten nanometres scale), and the formation of stronger H-bonds between water and TOCNFs (few Ångströms scale). In particular, in the case of TOCNFs 2% and Ca^{2+} ions, the effects on Kuhn length and H-bonds are more evident in the concentration range 2–5 mM, whereas the nanofibril swelling occurs at a concentration higher than 5 mM.

This study, clarifying the behaviour of TOCNF hydrogels at the nano and molecular scale, provides information that is essential for the comprehension of the even more complex interactions occurring when these systems are loaded with proteins or other macromolecules intended for biomedical applications.

Acknowledgments The authors thank Prof. Dr. Javier Martí-Rujas for his support in powder XRD analyses; the authors also thank Dr. Alberto Giacometti Schieroni, Daniele Piovani and Raniero Mendichi for their support for the rheological measurements.

Authors' contributions Conceptualization: Andrea Fiorati, Arianna Rossetti, and Carlo Punta. Methodology: Andrea Fiorati, Barbara Rossi, and Alessandro Paciaroni. Formal Analysis: Barbara Rossi, Lucia Comez, Silvia Corezzi, and Alessandro Paciaroni. Investigation: Arianna Rossetti, Cettina Bottari, and Andrea Fiorati. Resources: Carlo Punta. Writing—Original Draft: Arianna Rossetti and Andrea Fiorati. Writing—Review & Editing: All authors. Visualization: Andrea Fiorati. Supervision: László Almásy, Barbara Rossi, and Carlo Punta. Funding acquisition: Andrea Fiorati and Carlo Punta.

Funding Open access funding provided by Politecnico di Milano within the CRUI-CARE Agreement. The authors acknowledge the CERIC-ERIC Consortium for access to experimental facilities and financial support (proposal number 20182148).

Availability of data and materials Data available in attached SI file and on request to the corresponding author.

Declarations

Conflict of interest The authors declare no competing interests.

Consent for publication All authors revised the manuscript and agreed with the publication.

Ethics approval and consent to participate Not applicable.

References

Aaen R, Simon S, Wernersson Brodin F, Syverud K (2019) The potential of TEMPO-oxidized cellulose nanofibrils as rheology modifiers in food systems. Cellulose 26:5483–5496. https://doi.org/10.1007/s10570-019-02448-3

Almásy L (2021) New measurement control software on the yellow submarine SANS instrument at the budapest neutron centre. J Surf Investig X-Ray, Synchrotron Neutron Tech 15:527–531. https://doi.org/10.1134/S1027451021030046

Annabi N, Tamayol A, Uquillas JA et al (2014) 25th anniversary article: rational design and applications of hydrogels in regenerative medicine. Adv Mater 26:85–124. https://doi.org/10.1002/adma.201303233

Bonetti L, Fiorati A, D'Agostino A et al (2022) Smart methylcellulose hydrogels for pH-triggered delivery of silver nanoparticles. Gels 8:298. https://doi.org/10.3390/gels8050298

Bottari C, Comez L, Corezzi S et al (2017) Correlation between collective and molecular dynamics in pH-responsive cyclodextrin-based hydrogels. Phys Chem Chem Phys 19:22555–22563. https://doi.org/10.1039/C7CP04190J

Bottari C, Comez L, Paolantoni M et al (2018) Hydration properties and water structure in aqueous solutions of native and modified cyclodextrins by UV Raman and Brillouin scattering. J Raman Spectrosc 49:1076–1085. https://doi.org/10.1002/jrs.5372

Brannon-Peppas L, Peppas NA (1989) Solute and penetrant diffusion in swellable polymers. IX. The mechanisms of drug release from pH-sensitive swelling-controlled systems. J Control Release 8:267–274. https://doi.org/10.1016/0168-3659(89)90048-5

Celebi D, Guy RH, Edler KJ, Scott JL (2016) Ibuprofen delivery into and through the skin from novel oxidized cellulose-based gels and conventional topical formulations. Int J Pharm 514:238–243. https://doi.org/10.1016/j.ijpharm.2016.09.028

Coombs OBrien J, Torrente-Murciano L, Mattia D, Scott JL, (2017) Continuous production of cellulose microbeads via membrane emulsification. ACS Sustain Chem Eng 5:5931–5939. https://doi.org/10.1021/acssuschemeng.7b00662

Courtenay JC, Ramalhete SM, Skuze WJ et al (2018) Unravelling cationic cellulose nanofibril hydrogel structure: NMR spectroscopy and small angle neutron scattering analyses. Soft Matter 14:255–263. https://doi.org/10.1039/C7SM02113E

Crawford RJ, Edler KJ, Lindhoud S et al (2012) Formation of shear thinning gels from partially oxidised cellulose nanofibrils. Green Chem 14:300–303. https://doi.org/10.1039/C2GC16302K

da Silva PD, Montanari S, Vignon MR (2003) TEMPO-mediated oxidation of cellulose III. Biomacromol. https://doi.org/10.1021/bm034144s

De France KJ, Hoare T, Cranston ED (2017) Review of hydrogels and aerogels containing nanocellulose. Chem Mater 29:4609–4631. https://doi.org/10.1021/acs.chemmater.7b00531

Di Michele A, Freda M, Onori G et al (2006) Modulation of hydrophobic effect by cosolutes. J Phys Chem B 110:21077–21085. https://doi.org/10.1021/jp068055w

Diener M, Adamcik J, Bergfreund J et al (2020) Rigid, fibrillar quaternary structures induced by divalent ions in a carboxylated linear polysaccharide. ACS Macro Lett 9:115–121. https://doi.org/10.1021/acsmacrolett.9b00824

Dong H, Snyder JF, Williams KS, Andzelm JW (2013) Cation-induced hydrogels of cellulose nanofibrils with tunable moduli. Biomacromol 14:3338–3345. https://doi.org/10.1021/bm400993f

Eaves JD, Loparo JJ, Fecko CJ et al (2005) Hydrogen bonds in liquid water are broken only fleetingly. Proc Natl Acad Sci USA 102:13019–13022. https://doi.org/10.1073/pnas.0505125102

Fiorati A, Contessi Negrini N, Baschenis E et al (2020) TEMPO-nanocellulose/Ca2+ hydrogels: Ibuprofen drug diffusion and in vitro cytocompatibility. Materials (basel) 13:183. https://doi.org/10.3390/ma13010183

Fiorati A, Linciano C, Galante C et al (2021) Bioactive hydrogels: design and characterization of cellulose-derived injectable composites. Materials 14:4511. https://doi.org/10.3390/ma14164511

Fukuzumi H, Tanaka R, Saito T, Isogai A (2014) Dispersion stability and aggregation behavior of TEMPO-oxidized cellulose nanofibrils in water as a function of salt addition. Cellulose 21:1553–1559. https://doi.org/10.1007/s10570-014-0180-z

Geng L, Peng X, Zhan C et al (2017) Structure characterization of cellulose nanofiber hydrogel as functions of concentration and ionic strength. Cellulose 24:5417–5429. https://doi.org/10.1007/s10570-017-1496-2

Green JL, Lacey AR, Sceats MG (1986) Spectroscopic evidence for spatial correlations of hydrogen bonds in liquid water. J Phys Chem 90:3958–3964. https://doi.org/10.1021/j100408a027

Gu X, Mildner DFR (2016) Ultra-small-angle neutron scattering with azimuthal asymmetry. J Appl Crystallogr 49:934–943. https://doi.org/10.1107/S1600576716005586

Guccini V, Yu S, Agthe M et al (2018) Inducing nematic ordering of cellulose nanofibres using osmotic dehydration. Nanoscale 10:23157–23163. https://doi.org/10.1039/C8NR08194H

Habibi Y, Chanzy H, Vignon MR (2006) TEMPO-mediated surface oxidation of cellulose whiskers. Cellulose 13:679–687. https://doi.org/10.1007/s10570-006-9075-y

Heinze T, el Seoud OA, Koschella A (2018) Cellulose derivatives: synthesis, structure, and properties. Springer Cham, USA

Hoffman AS (2012) Hydrogels for biomedical applications. Adv Drug Deliv Rev 64:18–23. https://doi.org/10.1016/j.addr.2012.09.010

Hua K, Rocha I, Zhang P et al (2016) Transition from bioinert to bioactive material by tailoring the biological cell response to carboxylated nanocellulose. Biomacromol 17:1224–1233. https://doi.org/10.1021/acs.biomac.6b00053

Isogai A, Saito T, Fukuzumi H (2011) TEMPO-oxidized cellulose nanofibres. Nanoscale 3:71–85. https://doi.org/10.1039/C0NR00583E

Jha PK, Zwanikken JW, de la Cruz M (2012) Understanding swollen–collapsed and re-entrant transitions in polyelectrolyte nanogels by a modified Donnan theory. Soft Matter 8:9519–9522. https://doi.org/10.1039/C2SM26341F

Joachimiak A, Halamus T, Wojciechowski P, Ulanski J (2005) Structure of hydrogels based on lyotropic phases of cellulose derivative as studied by Raman spectroscopy. Macromol Chem Phys 206:59–65. https://doi.org/10.1002/macp.200400132

Keiderling U (2002) The new 'BerSANS-PC' software for reduction and treatment of small angle neutron scattering data. Appl Phys A 74:s1455–s1457. https://doi.org/10.1007/s003390201561

Lan G-X, Liu Y, Zhou N et al (2022) Multifunctional nanocellulose-based composites for potential environmental applications. Cellulose. https://doi.org/10.1007/s10570-022-04918-7

Li L (2002) Thermal gelation of methylcellulose in water: scaling and thermoreversibility. Macromolecules 35:5990–5998. https://doi.org/10.1021/ma0201781

Lippi M, Riva L, Caruso M, Punta C (2022) Cellulose for the production of air-filtering systems: a critical review. Materials 15:976. https://doi.org/10.3390/ma15030976

Maeda Y, Kitano H (1995) The structure of water in polymer systems as revealed by Raman spectroscopy. Spectrochim Acta Part A Mol Biomol Spectrosc 51:2433–2446. https://doi.org/10.1016/0584-8539(95)01446-2

Mao Y, Liu K, Zhan C et al (2017) Characterization of nanocellulose using small-angle neutron, X-ray, and dynamic light scattering techniques. J Phys Chem B 121:1340–1351. https://doi.org/10.1021/acs.jpcb.6b11425

Marinov VS, Nickolov ZS, Matsuura H (2001) Raman spectroscopic study of water structure in aqueous nonionic surfactant solutions. J Phys Chem B 105:9953–9959. https://doi.org/10.1021/jp011936c

Masruchin N, Kurniawan YD, Kusumah SS et al (2019) TEMPO-mediated oxidation cellulose pulp modified with Monosodium Glutamate (MSG). IOP Conf Ser Earth Environ Sci 374:12010. https://doi.org/10.1088/1755-1315/374/1/012010

Mauri E, Micotti E, Rossetti A et al (2018) Microwave-assisted synthesis of TEMPO-labeled hydrogels traceable with MRI. Soft Matter 14:558–565. https://doi.org/10.1039/c7sm02292a

Mauri E, Naso D, Rossetti A et al (2019) Design of polymer-based antimicrobial hydrogels through physico-chemical transition. Mater Sci Eng C 103:109791. https://doi.org/10.1016/j.msec.2019.109791

Mendoza L, Batchelor W, Tabor RF, Garnier G (2018) Gelation mechanism of cellulose nanofibre gels: A colloids and interfacial perspective. J Colloid Interface Sci 509:39–46. https://doi.org/10.1016/j.jcis.2017.08.101

Miao C, Hamad WY (2013) Cellulose reinforced polymer composites and nanocomposites: a critical review. Cellulose 20:2221–2262. https://doi.org/10.1007/s10570-013-0007-3

Paolantoni M, Lago NF, Albertí M, Laganà A (2009) Tetrahedral ordering in water: Raman profiles and their temperature dependence. J Phys Chem A 113:15100–15105. https://doi.org/10.1021/jp9052083

Pastorczak M, Kozanecki M, Ulanski J (2009) Water-polymer interactions in PVME hydrogels – Raman spectroscopy studies. Polymer 50:4535–4542. https://doi.org/10.1016/j.polymer.2009.07.048

Pedersen JS, Schurtenberger P (1996) Scattering functions of semiflexible polymers with and without excluded volume effects. Macromolecules 29:7602–7612. https://doi.org/10.1021/ma9607630

Pierre G, Punta C, Delattre C et al (2017) TEMPO-mediated oxidation of polysaccharides: an ongoing story. Carbohydr Polym 165:71–85. https://doi.org/10.1016/j.carbpol.2017.02.028

Pitton M, Fiorati A, Buscemi S et al (2021) 3D Bioprinting of pectin-cellulose nanofibres multicomponent bioinks. Front Bioeng Biotechnol 9:732689

Quennouz N, Hashmi SM, Choi HS et al (2016) Rheology of cellulose nanofibrils in the presence of surfactants. Soft Matter 12:157–164. https://doi.org/10.1039/C5SM01803J

Rashad A, Mustafa K, Heggset EB, Syverud K (2017) Cytocompatibility of wood-derived cellulose nanofibril hydrogels with different surface chemistry. Biomacromol 18:1238–1248. https://doi.org/10.1021/acs.biomac.6b01911

Ratajska-Gadomska B, Gadomski W (2004) Water structure in nanopores of agarose gel by Raman spectroscopy. J Chem Phys 121:12583–12588. https://doi.org/10.1063/1.1826051

Riva L, Fiorati A, Punta C (2021) Synthesis and application of cellulose-polyethyleneimine composites and nanocomposites: a concise review. Materials 14:473. https://doi.org/10.3390/ma14030473

Rossi B, Venuti V, D'Amico F et al (2015a) Water and polymer dynamics in a model polysaccharide hydrogel: the role of hydrophobic/hydrophilic balance. Phys Chem Chem Phys 17:963–971. https://doi.org/10.1039/C4CP04045G

Rossi B, Venuti V, D'Amico F et al (2015b) Toward an understanding of the thermosensitive behaviour of pH-responsive hydrogels based on cyclodextrins. Soft Matter 11:5862–5871. https://doi.org/10.1039/C5SM01093D

Rossi B, Bottari C, Comez L et al (2018) Structural and molecular response in cyclodextrin-based pH-sensitive

hydrogels by the joint use of Brillouin, UV Raman and small angle neutron scattering techniques. J Mol Liq 271:738–746. https://doi.org/10.1016/j.molliq.2018.08.141

Rossi B, Bottari C, Catalini S, et al (2020) Chapter 13 - Synchrotron-based ultraviolet resonance Raman scattering for material science. In: Gupta VP, Ozaki YBT-M and LS (eds) Molecular and laser spectroscopy. Advances and Applications: Volume 2. Elsevier, USA, pp 447–482.

Saito T, Isogai A (2004) TEMPO-mediated oxidation of native cellulose. The effect of oxidation conditions on chemical and crystal structures of the water-insoluble fractions. Biomacromol 5:1983–1989. https://doi.org/10.1021/bm0497769

Saito T, Kimura S, Nishiyama Y, Isogai A (2007) Cellulose nanofibres prepared by TEMPO-mediated oxidation of native cellulose. Biomacromol 8:2485–2491. https://doi.org/10.1021/bm0703970

Saito T, Uematsu T, Kimura S et al (2011) Self-aligned integration of native cellulose nanofibrils towards producing diverse bulk materials. Soft Matter 7:8804–8809. https://doi.org/10.1039/C1SM06050C

Sassi P, Paolantoni M, Cataliotti RS et al (2004) Water/alcohol mixtures: a spectroscopic study of the water-saturated 1-octanol solution. J Phys Chem B 108:19557–19565. https://doi.org/10.1021/jp046647d

Schneider CA, Rasband WS, Eliceiri KW (2012) NIH image to image J: 25 years of image analysis. Nat Methods. https://doi.org/10.1038/nmeth.2089

Sharp P, Bloomfield VA (1968) Light scattering from wormlike chains with excluded volume effects. Biopolymers 6:1201–1211. https://doi.org/10.1002/bip.1968.360060814

Sing CE, Zwanikken JW, Olvera de la Cruz M (2013) Effect of ion-ion correlations on polyelectrolyte gel collapse and reentrant swelling. Macromolecules 46:5053–5065. https://doi.org/10.1021/ma400372p

Stanislas TT, Bilba K, de Oliveira Santos RP et al (2022) Nanocellulose-based membrane as a potential material for high performance biodegradable aerosol respirators for SARS-CoV-2 prevention: a review. Cellulose 29:8001–8024. https://doi.org/10.1007/s10570-022-04792-3

Su Y, Burger C, Hsiao BS, Chu B (2014) Characterization of TEMPO-oxidized cellulose nanofibres in aqueous suspension by small-angle X-ray scattering. J Appl Crystallogr 47:788–798. https://doi.org/10.1107/S1600576714005020

Tanpichai S, Boonmahitthisud A, Soykeabkaew N, Ongthip L (2022) Review of the recent developments in all-cellulose nanocomposites: properties and applications. Carbohydr Polym 286:119192. https://doi.org/10.1016/j.carbpol.2022.119192

Ullah F, Othman MBH, Javed F et al (2015) Classification, processing and application of hydrogels: a review. Mater Sci Eng C 57:414–433. https://doi.org/10.1016/j.msec.2015.07.053

Valencia L, Nomena EM, Monti S et al (2020) Multivalent ion-induced re-entrant transition of carboxylated cellulose nanofibrils and its influence on nanomaterials' properties. Nanoscale 12:15652–15662. https://doi.org/10.1039/D0NR02888F

Vismara I, Papa S, Veneruso V et al (2020) Selective modulation of A1 astrocytes by drug-loaded nano-structured gel in spinal cord injury. ACS Nano 14:360–371. https://doi.org/10.1021/acsnano.9b05579

Walrafen GE (1967) Raman spectral studies of the effects of temperature on water structure. J Chem Phys 47:114–126. https://doi.org/10.1063/1.1711834

Zemb T, Lindner P (2002) Neutron. X-rays and Light. Scattering Methods Applied to Soft Condensed Matter, Elsevier, North Holland

Zou P, Yao J, Cui Y-N et al (2022) Advances in cellulose-based hydrogels for biomedical engineering: a review summary. Gels 8:364. https://doi.org/10.3390/gels8060364